Springer Proceedings in Physics 247

Olena Fesenko
Leonid Yatsenko *Editors*

Nanooptics and Photonics, Nanochemistry and Nanobiotechnology, and Their Applications

Selected Proceedings of the 7th International Conference Nanotechnology and Nanomaterials (NANO2019), 27–30 August 2019, Lviv, Ukraine

Springer

Mechanisms of Antitumor Effect of Nanomaterials Based on Rare Earth Orthovanadates

Anatoliy Goltsev, Yurii Malyukin, Natalya Babenko, Yuliya Gaevska, Mykola Bondarovych, Igor Kovalenko, Tatiana Dubrava, and Vladimir Klochkov

1 Introduction

According to the World Health Organization's data in 2018, cancer has caused 9 million deaths worldwide within the reporting period and is expected to increase

A. Goltsev (✉) · N. Babenko · Y. Gaevska · M. Bondarovych · T. Dubrava
Department of Cryopathophysiology and Immunology, Institute for Problems of Cryobiology & Cryomedicine of the National Academy of Sciences of Ukraine, Pereyaslavska Street 23, 61016 Kharkiv, Ukraine
e-mail: cryopato@gmail.com

N. Babenko
e-mail: natybabenko@gmail.com

Y. Gaevska
e-mail: yugaevska@gmail.com

M. Bondarovych
e-mail: nikolay.bondarovicg@gmail.com

T. Dubrava
e-mail: tgdubrava@gmail.com

Y. Malyukin · V. Klochkov
Department of Nanocrystal Materials, Institute for Scintillation Materials of the National Academy of Sciences of Ukraine, 60 Nauki Avenue, 61001 Kharkiv, Ukraine
e-mail: maljukin@nas.gov.ua

V. Klochkov
e-mail: klochkov@isma.kharkov.ua

I. Kovalenko
Department for Low Temperature preservation, Institute for Problems of Cryobiology & Cryomedicine of the National Academy of Sciences of Ukraine, Pereyaslavska Street 23, 61016 Kharkiv, Ukraine
e-mail: i.kovalenko.ipcic@gmail.com

O. Fesenko and L. Yatsenko (eds.), *Nanooptics and Photonics, Nanochemistry*

up to 22 million by 2035 [1]. Modern cancer treatments include surgery, radiation and chemotherapy, the main drawback of those is their non-specificity. Conventional chemotherapeutic agents have no deliberate action and affect both cancer and normal cells, thereby leading to non-optimal treatment as a result of excessive toxicity.

Targeted therapy using a variety of nanomaterials has become one of the means of overcoming the lack of specificity to tumor cells of conventional chemotherapy drugs. Due to the tremendous efforts that have been made in nanomedicine over the past decades, several therapeutic strategies have been proposed to treat oncopathology, including photothermal ablation therapy using silicon nanoshells [2], carbon nanotubes [3], gold nanorods [4]. In addition, nanoparticles (NPs) are used for targeted delivery of antitumor agents [5].

Successful use of NPs in the clinic requires their specific design with adapted properties for safer and more effective cancer treatment. A significant advantage of inorganic gadolinium and yttrium orthovanadate nanoparticles is their high biocompatibility and ability to simultaneously target tumor cells and inhibit their function. When studying the toxicity, the dynamics of accumulation and excretion of NPs based on orthovanadates, it has been found that their oral and intraperitoneal administration to rats did not lead to the death of animals and a change in the mass coefficients of internal organs, which made it possible to attribute the synthesized samples of nanovanadates to practically nontoxic compounds (toxicity class V). Complete excretion of NPs from the body occurred 30 days after administration [6]. Low IC50 (half maximal inhibitory concentration) of vanadium compounds [7] supports the evidence of the absence of toxic effects of vanadium (IV) on normal non-cancerous cells [8].

Owing to its atomic mass (Mr = 64), gadolinium is a good electron emitter, which greatly enhances radiation-induced destruction of cells previously sensitized by nanoparticles [9]. In addition, the NPs based on rare-earth metals have photophysical properties, including a high photostability for a long time, a significant Stokes shift of luminescence, the absence of flicker, the stability of characteristic narrow luminescence bands, that opens up the prospect of their use as luminescent labels and probes [10].

As reported [11] the antitumor effect of some organic derivatives of vanadium [V (IV)] (bis (maltolato) oxovanadium (IV), bis (coyato) oxovanadium (IV) and bis 2,2′-bipyridine) oxovanadium (IV) sulfate was shown, the addition of which to the culture of H-35 tumor cells at a concentration of 0.5–5.0 mM led to significant inhibition of its growth and proliferation. Vanadyl sulfate [V (IV)] or vanadate [V (V)] had a similar effect on tumor cells [12].

Vanadium compounds can cause selective oxidation of pyrimidine bases, which prevents a complementary DNA folding [13]. The tumor cells, characterized by the disorders of the DNA repair system, are especially subjected to it. Another proposed mechanism for the antitumor effect of vanadium compounds is their impaired permeability of the tumor cell mitochondrial membrane as a result of generation of reactive oxygen species [14], that leads to a release of cytochrome C and induction of apoptosis [15].

However, elucidation of the conditions and mechanisms for implementation of the ability of NPs based on rare-earth orthovanadates to change the proliferative and metabolic activity of tumor cells has remained an urgent task.

Targeted accumulation of nanoparticles in tumor cells can be achieved by modifying them and creating on their base of nanoemulsions, namely combining them with cholesterol [16]. It is known that cancer cells, with high metabolic activity, are able to selectively capture cholesterol from a biological environment [17]. Therefore, cholesterol supplementation is a prerequisite for successful targeted delivery to tumor sites. They are kinetically stable dispersion systems, resistant to stratification for several months. In addition, the nanoemulsion of cholesterol is relatively resistant to reactive oxygen species, which allows a long-term circulation of cholesterol in the bloodstream [16].

The purpose of this study was to investigate the possibility of using $GdYEuVO_4$ nanoparticles and hybrid nanocomplexes synthesized on their basis to visualize and use in the treatment of malignant tumors.

2 Physico-Chemical Characteristics of Nanomaterials Based on Rare-Earth Orthovanadates

2.1 Synthesis of Aqueous Solutions of $GdYEuVO_4$ Nanoparticles

Aqueous solutions of nanoparticles based on $Gd_{0.7}Y_{0.2}Eu_{0.1}VO_4$ rare-earth orthovanadates were obtained by colloidal synthesis [18]. In brief: in a 50 ml flask, 1 M aqueous solutions of rare-earth chlorides (Sigma Aldrich) were mixed: gadolinium chloride 0.35 ml, 0.1 ml yttrium chloride and 0.05 ml europium chloride, then the solution was added with bidistilled water to the mark. After this, the resulting solution was mixed with the one of sodium citrate (37.5 ml, 0.01 mol/l). Then, an aqueous solution of sodium orthovanadate (37.5 ml, 0.01 mol/l) was added dropwise to the resulting mixture using a magnetic stirrer. The pH of the resulting solution was adjusted with hydrochloric acid to 10.5. Then the reaction mixture was heated in a thermostat at 60 °C for 90 min.

After finishing heat treatment and cooling, the solution was dialyzed through a 12 kDa membrane (pore size made 2.5 nm). The dialysis lasted for 3 days, however, every 6 h the distilled water was replaced in a glass. The cleaning of the dialyzed solution from electrolyte impurities was monitored by determining the dialysate electrical conductivity. Concentrated solutions were obtained by evaporation with a rotary evaporator at 60 °C.

The applied colloidal synthesis technique allows the obtaining of aggregatively stable hydrosols of nanoparticles (NPs) with controlled geometric parameters of a solid phase. The absence in the aqueous solutions of nanoparticles of toxic impurities,

surfactants and polymers that are able to interact with biological objects makes them suitable for biological testing.

2.2 *Characterization of Aqueous Solutions of $GdYEuVO_4$ Nanoparticles*

Like typical colloidal systems, the studied aqueous solutions of NPs are transparent in transmitted light and opalescent under lateral illumination (Tyndall cone is observed).

Under UV irradiation, aqueous solutions of NPs exhibit bright red luminescence. Their pH value is within the range of 7.4–7.8. The ζ potential of NPs in colloidal solutions was measured using a ZetaPALS analyzer (Brookhaven Instruments Corp., USA) at a 15° scattering angle. In calculating the ζ potential, the Doppler shift of the beam of light scattered by the particles was measured, followed by recalculation according to the Smoluchowski equations. The value of ζ potential may be -36 ± 4 mV, depending on the type of NPs and storage time.

Colloidal solutions of NPs easily pass through nitrocellulose ultrafilters with a pore diameter of 100 nm. The solid phase concentration of aqueous solutions of NPs is 1.3 g/L. The resulting solutions can be stored for more than 6 months under standard conditions without changing their properties. Sterilization of NPs solutions at 120 °C for 1–2 h in the sealed ampoules does not cause sedimentation and coagulation of colloids.

The size and morphology of the NPs were evaluated using transmission electron microscopy (TEM) with a 125K TEM electron microscope (Selmi, Ukraine) at an accelerating voltage of 100 kV (magnification up to ×100,000). For studies in a transmission mode, the samples were prepared according to the standard method by applying a colloidal solution to copper grids coated with a thin layer of carbon, followed by drying at room temperature.

The method of TEM showed that the NPs had a spherical shape with an average diameter of 3 nm (Fig. 1). Size dispersion did not exceed 15%.

To obtain the absorption spectra, a SPECORD 200 spectrophotometer (Analytik-Jena, Germany) was used by means of both single-beam and double-beam schemes. The absorption spectra of aqueous solutions of NPs exhibit a broadband with a maximum of 271 nm, which corresponds to optical transitions with charge transfer from oxygen ligands to the central vanadium ion in VO_4^3 (Fig. 2). It is worthy of noting that for ionic solutions of salts containing VO_4^{3-} ions, the absorption maximum is in the region of $\lambda_{max} = 266$ nm, a shift of this band to the long-wavelength region indicates that VO_4^{3-} is in the crystalline field.

The dependence of an optical density on the concentration of NPs is linear in the studied concentration range of 5×10^{-5}–1×10^{-3} mol/l (0.01–0.25 g/l), which indicates the compliance with the Bouguer–Lambert–Beer absorption law for these systems. The values of the absorption maximum are used to determine the concentration of NPs in solutions [19].

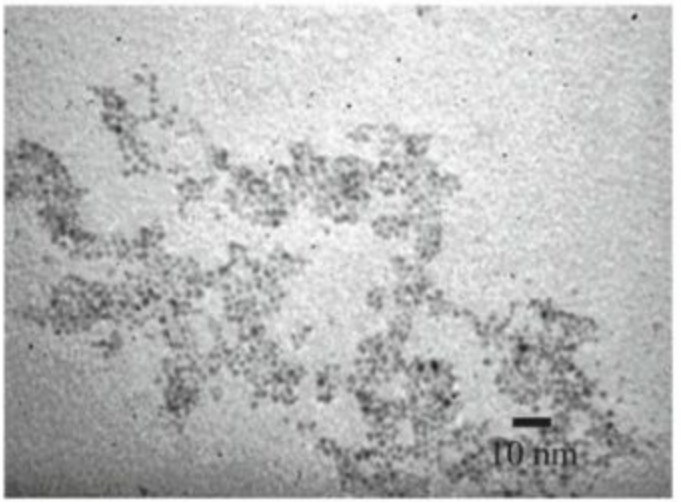

Fig. 1 TEM image of solid phase of aqueous solution of $GdYEuVO_4$ nanoparticles

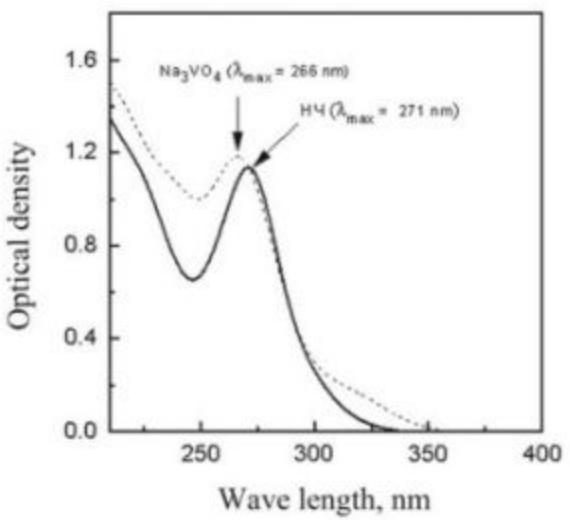

Fig. 2 Absorption spectra of Na_3VO_4 solution and aqueous solution of $GdYEuVO_4$ nanoparticles

Luminescence spectra were measured with a Lumina spectrophotometer (ThermoScientific, USA). An intense band was observed in the luminescence excitation spectrum of an aqueous solution of $GdYEuVO_4$ nanoparticles, which coincided with the absorption band, as well as several low-intensity narrow lines in the longer wavelength region (395, 465, 536 nm) corresponding to optical f–f transitions of europium in the orthovanadate matrix (Fig. 3). The absorption intensity of f–f transitions of Eu^{3+} is very weak when compared with the absorption if the VO_4^3 group, indicating

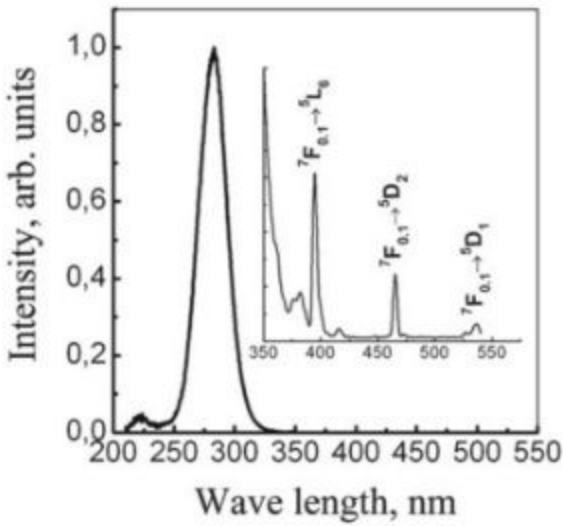

Fig. 3 Luminescence excitation spectrum (λ = 270 nm) of an aqueous solution of $GdYEuVO_4$ nanoparticles. Insert An enlarged image of bands in visible region of spectrum

that excitation of Eu^{3+} ions, mainly through VO_4^3 groups, that is, by transferring energy from the VO_4^3 group to Eu^{3+} ions. It should be noted that during the matrix excitation (270 nm), the Stokes shift exceeds 300 nm, which provides visual contrast and separation of the luminescence of NPs from the autoluminescence of cells during testing.

The luminescence spectrum (Fig. 4) of the studied aqueous solution of $GdYEuVO_4$ nanoparticles is represented by narrow bands of the $^5D_0 \rightarrow {}^7F_J$ transitions ($J = 0, 1, 2, 3, 4$), characteristic of the europium ion in the composition of orthovanadate matrix. The most intense peaks are observed at the $^5D_0$–$^7F_2$ electric dipole transition at 615 and 618 nm. The band corresponding to the $^5D_0$–$^7F_4$ electric dipole transition contains narrow lines with maxima of 698 and 704 nm. At 650 nm, weak lines are observed corresponding to the $^5D_0$–$^7F_3$ magnetic dipole transition. Narrow lines and their fine structure confirm the crystalline nature of NPs. The presence of these bands within a visible range allows the identification and registration of NPs using luminescence microscopy in experiments in vitro and in vivo.

It has been established that in biological environments of the NPs, based on orthovanadates of the rare-earth elements are not inert. They are often subjected to aggregates and/or agglomeration, especially in salines, that may lead to formation of new molecular complexes [20]. To stabilize the NPs, the isotonic solution of 5% glucose was used as a solvent, since previous studies have demonstrated no changes in the NPs diameter occur under these conditions, that is a strong advantage for further investigations in biosystems.

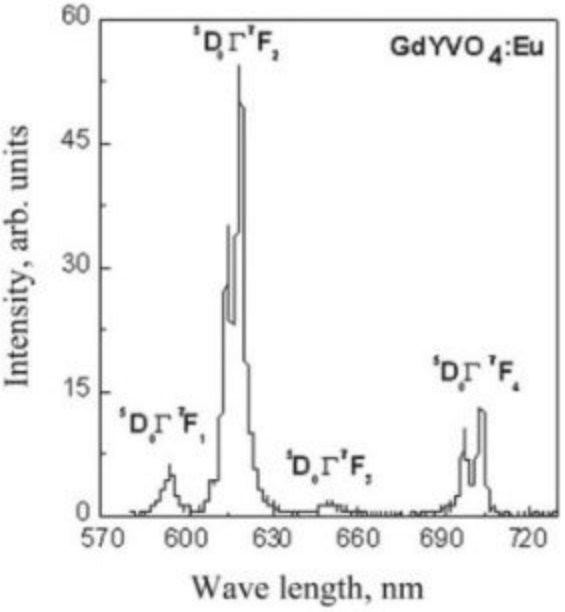

Fig. 4 Luminescence spectrum ($\lambda = 618$ nm) of aqueous solution of $GdYEuVO_4$ nanoparticles

2.3 *Synthesis and Physicochemical Properties of Hybrid Nanocomplexes*

A hybrid nanocomplexes (NCs) is an aqueous dispersion of sheep cholesterol in concentration of 0.55 g/l (Acros organics, Belgium) using $GdYEuVO_4$ nanoparticles (of 2–3 nm diameter) at a concentration of 1.30 g/l. Hybrid nanocomplexes were first synthesized at the Institute for Scintillation Materials of the National Academy of Sciences of Ukraine (Kharkiv) as reported [16]. A method of eliminating the NCs involves dissolving the cholesterol in ethyl alcohol and adding to the mixture a stabilizer substance, stirring the mixture with subsequent evaporation with a rotary evaporator. The use of NPs above 5 nm reduces the probability of their localization on the surface of the dispersed cholesterol particles and does not provide sufficient electrokinetic potential (charge) on the surface of the dispersed cholesterol particles for their electrostatic repulsion in solution, and therefore does not contribute to their aggregation.

In hybrid NCs the negatively charged NPs are localized along the periphery of cholesterol particles owing to van der Waals and hydrophobic interactions. The NPs stabilize the hybrid NCs via electrostatic interactions. The sizes of the synthesized NCs do not exceed 100 nm. Negatively charged hybrid NPs of orthovanadates interfere an adhesion and aggregation of cholesterol particles. Structure of hybrid NCs is shown in Fig. 5.

The ideology of using such hybrid NCs in cancer therapy is based on the assumption that the antitumor effect of each of its components is mutually reinforced

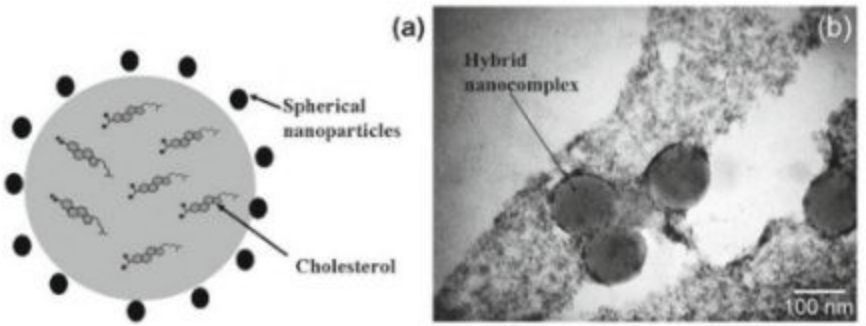

Fig. 5 Hybrid nanocomplex: **a** schematic representation, **b** transmission electron microscopy photomicrography of hybrid nanocomplexes, procured from cholesterol aqueous solution placed on carbon network

due to the presence of cholesterol in them, which has an affinity for the tumor cell membranes with a simultaneous possibility of their identification due to the luminescent properties of orthovanadates NPs [16].

It is known that cholesterol is actively "eliminated" from the bloodstream by proliferating cancer cells to build biomembranes. This is facilitated by the presence on the surface of tumor cells of a large number of SR-B1 (scavenger receptor, class B type I) and caveolin-1 (Cav-1) receptors that can bind to free cholesterol from the bloodstream [17]. Thus, the incorporation of cholesterol into the membranes of tumor cells can serve as a prerequisite for targeted delivery of hybrid NCs directly into a cell.

3 The Ways to Inhibit the Tumor Growth by Using Nanomaterials Based on Rare-Earth Orthovanadates

The possibility of nanomaterials based on $GdYEuVO_4$ rare-earth orthovanadates to identify and specifically inhibited the tumor-inducing cells should, first of all, be assessed under adequate experimental conditions. A convenient model for performing such experimental research is the inoculated tumor cell line of Ehrlich carcinoma (EC), which was obtained from spontaneous breast cancer in mice [21]. The EC tumor cell inoculation is 100%.

According to the histological structure, the EC is an undifferentiated tumor that has lost its epithelial character. Ehrlich carcinoma exists in the form of two strains, i.e., subcutaneous and ascites. The average life span of animals with the ascites EC induced by intraperitoneal injection of 3×10^6 cells/mouse is 10–16 days, and with subcutaneous inoculation, it makes 16–20 days [21]. Such properties of EC as growth rate, good reproducibility, and the relative constancy of morphological and biological properties make it possible to use it in experimental oncology.

Previous assessment of phenotypic characteristics and functional potential of the ascites EC has shown that this tumor is a heterogeneous population of tumor cells of various degrees of differentiation, related to highly and less potent tumor-inducing precursors [22]. In general, the differentiation row of subpopulations of breast cancer cells can be represented as follows:

$$CD44^{high} \rightarrow CD44^{+}CD24^{-} \rightarrow CD44^{+}CD24^{+} \rightarrow CD44^{-}CD24^{+}$$

At the same time, a higher (10-fold) tumorigenic activity of $CD44^{+}$ cells of EC in comparison with $CD44^{-}$ cells has been proven. In the compared pair, $CD44^{+}$ cells had a higher potential to form subpopulations of $CD44^{high}$, $CD44^{+}CD24^{-}$ and $CD44^{+}CD24^{+}$ cells in peritoneal cavity (PC) of mice, emphasizing the presence of stem cancer cells in the $CD44^{+}$ population [22].

Thus, an excellent inoculation, easy reproducibility, and analysis of the EC subpopulation composition suggest its successful use in testing new drugs, including nanomaterials. It has been previously shown that the NPs of rare-earth orthovanades of various shapes and sizes (spherical, spindle-like, and rod-like) had different binding potentials for the EC tumor cells in vitro. Spectral analysis demonstrated that NPs of only spherical and spindle-shaped forms can identify the tumor cells in the total pool of EC [23].

The question on the duration of interaction of tumor cells with nanomaterials remains unclear since, in these studies, the incubation time was selected according to the data obtained from healthy liver cells [24]. The most informative way to find out the dynamics of the accumulation of nanomaterials inside a cell is to use a multispectral analysis using a laser scanning microscope. The capabilities of a conventional fluorescence microscope are limited and it is safe to say that NPs are on or inside the cell surface. On the contrary, using the optical slicing method and subsequent 3D reconstruction of the object, it is possible to reproduce the volume distribution of nanomaterials in a cell and to evaluate the results of studies in four dimensions: length, width, depth and time.

Therefore, the number of cells that bind to NPs and hybrid NCs was counted using an LSM 510 META confocal laser scanning microscope (Carl Zeiss, Germany) after different incubation periods (1, 2, 3, and 4 h). The results of the study showed that the EC cells without the addition of nanomaterials (Control) throughout the observation period had an average fluorescence intensity of 15.33 ± 3.28 arb. units corresponding to an electronic noise level of the detector (Fig. 6).

Confocal microscopy showed a gradual penetration and accumulation of NPs in the EC cells during the study time period (1–4 h) (Figs. 6a, 7). After 1 h of incubation, an increase in mean fluorescence intensity (97.73 ± 10.13 arb. units) was found in all the EC cells compared to the control (15.33 ± 3.28 arb. units), which indicates the penetration of NPs inside cells. After 2 h of incubation, average fluorescence intensity of total pool of the EC cells continued to increase (125.33 ± 20.28 arb. units) and reached a maximum by 3 h (177.27 ± 24.50 arb. units). At this time single cells with hyperhigh ($2.220.50 \pm 119.50$ arb. units), which did not exceed 5% appeared. After 4 h of incubation, the mean fluorescence intensity of the total cell

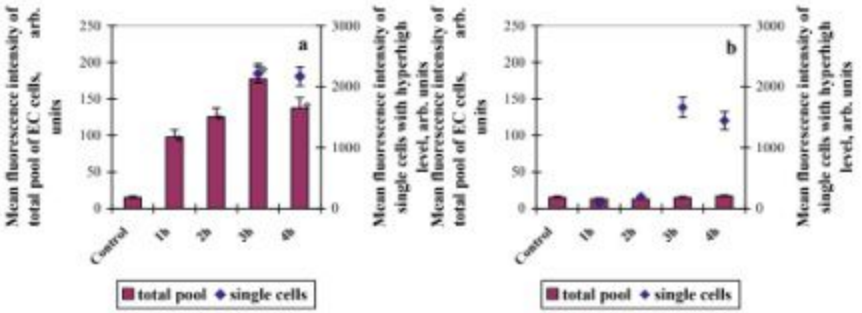

Fig. 6 Mean fluorescence intensity of total EC cell population (rectangular columns) and fluorescence of individual cells (blue marker) after incubation with spherical NPs (**a**) and hybrid NCs (**b**) for 1, 2, 3 and 4 h. *Note* Asterisk—difference is statistically significant compared with similar indices of EC cells without incubation with NPs or NCs (control) ($p < 0.05$)

population decreased slightly (137.75 ± 14.84 arb. units), with the number of single cells with a hyperhigh degree of luminescence remaining at the same level (2172 ± 110.70 arb. units) as after 3 h incubation.

Thus, NPs have been shown to be able to penetrate and accumulate in virtually all cells in total EC pool. The maximum accumulation of NPs in tumor cells is established after their 3-hour incubation. In the same period, the single cells with hyperhigh level of fluorescence appeared, the number of which did not exceed 5%. This indicates that NPs have the ability to identify all the tumor cells. The intensity of intracellular accumulation of NPs was different. Only a small population of tumor cells was capable of increased accumulation of the NPs under study.

Unlike NPs, the incubation of EC cells with hybrid NCs within the whole observation period practically did not change the mean fluorescence intensity of the total pool of cells compared to the control (Figs. 6b, 7). However, starting from the first hour of incubation, the appearance of individual cells with an extremely high level of fluorescence intensity (89 ± 5.72 arb. units), which reached maximum values after 3 h of incubation (1662 ± 33.89 arb. units), was noted (Fig. 6b). At the 4th hour of incubation, the fluorescence intensity of single cells with hyperhigh levels did not change significantly, remaining at a fairly high level (1445 ± 11.70 arb. units). The number of cells with hyperhigh fluorescence intensity gradually increased during the observation time, from 0.2% in the first hour to 1% of the total number of cells in a vision field at 3 h of incubation, remaining at this level until the end of the observation period.

Thus, the hybrid NCs have been established to be able of selective binding only to individual tumor cells, the number of which did not exceed 1% in the absence of their accumulation in total population of EC cells.

To determine to which EC population on phenotypic signs the cells with high levels of fluorescence belong were simultaneously treated with the cells with nanomaterials and monoclonal antibodies to CD44 (Fig. 8). The incubation period of cells with hybrid NCs and NPs with double staining was 3 h according to the above data on the

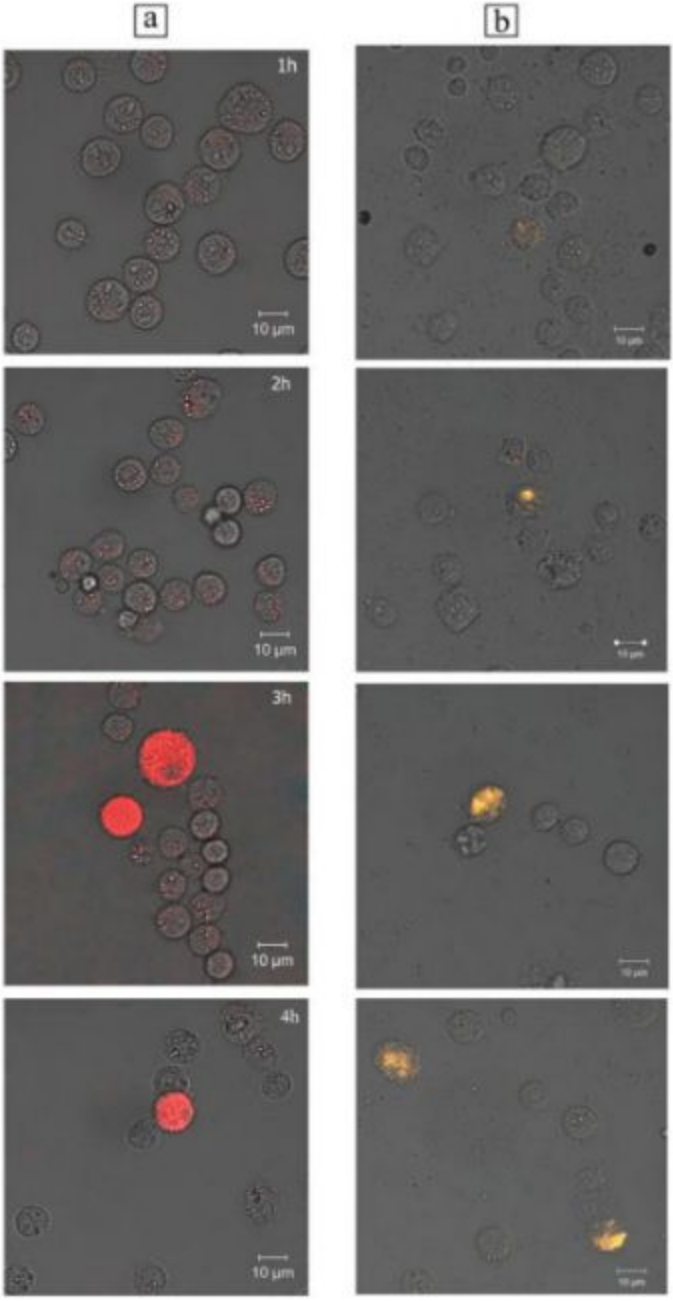

Fig. 7 Confocal microscopy of EC cells after incubation with spherical NPs (**a**) and hybrid NCs (**b**) for 1, 2, 3, and 4 h

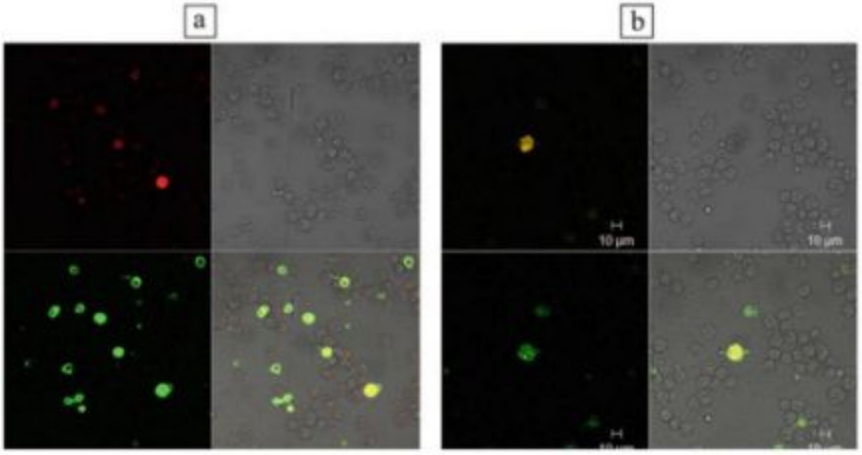

Fig. 8 Double staining of EC cells with nanomaterials—red and yellow fluorescence and monoclonal antibodies to CD44—green fluorescence (**a** treatment with spherical nanoparticles, **b** treatment with hybrid nanocomplexes). Confocal microscopy of EC cells after 3 h incubation with nanomaterials

maximum accumulation of nanomaterials during exactly this period. The rationale for this approach was the previously established fact that it is $CD44^+$ cells that have a proliferative potential, estimated by the tumor growth rate in vivo, and play a critical role in tumorigenesis [22].

Confocal microscopy data confirmed (Table 1) that the number of $CD44^+$ cells with green fluorescence was $7.00 \pm 0.58\%$ of the total EC pool. However, these cells were found to have different levels of fluorescence intensity. Thus, $5.83 \pm 0.63\%$ of $CD44^+$ cells had a fluorescence intensity of 300.25 ± 96 arb. units. At that time, only $1.17 \pm 0.10\%$ of $CD44^+$ cells had ultra-high fluorescence (1297.29 ± 46 arb. units) and can be attributed to $CD44^{high}$ cells. It is well known that they are stem cancer cells and have the highest tumor-inducing potential [22].

Table 1 Fluorescence intensities of EC cells after their double staining with monoclonal antibodies to CD44 and nanomaterials

	Number of cells with fluorescence versus total EC pool (%)		
	Staining type		
	CD44	CD44 + NPs	CD44 + NCs
Fluorescence intensity (arb. units)	7.00 ± 0.58	6.74 ± 0.41	1.20 ± 0.13
With the highest fluorescence (%)	1.17 ± 0,10	5.16 ± 0.41	1.20 ± 0.13
Fluorescence intensity (arb. units)	1297.29 ± 46	2220.50 ± 119.50	1662.49 ± 33.89
With mean fluorescence (%)	5.83 ± 0.63	2.04 ± 0.17	–
Fluorescence intensity (arb. units)	300.25 ± 96	177.27 ± 24.50	–

The double staining of EC cells by nanoparticles and monoclonal antibodies to CD44 was found to be characteristic of 6.74 ± 0.41% of total EC pool cells. This indicates that NPs are capable of accumulating in almost all the cells expressing the CD44 marker (Fig. 8a, Table 1). The vast majority of $CD44^+$ cells (76.56%) were capable of intense NPs accumulation, as evidenced by their ultra-high fluorescence level of this marker (2220.50 ± 119.50 arb. units). The number of cells with mean NPs fluorescence was about one-third of the entire $CD44^+$ population. It was noted that this level had no statistically significant differences from the fluorescence level of cells in total EC pool capable of accumulating NPs. Thus, the NPs were found to have some affinity to $CD44^+$ cells, but not absolute, due to their presence in the vast majority of cells lacking the CD44 marker.

Figure 8 demonstrated the difference in a selective accumulation of NPs and hybrid NCs in CD44 population. It is quite illustrative. Thus, unlike NPs, the accumulation of hybrid NCs was observed only in 1.20 ± 0.13% of cells in a total pool of EC (Table 1). At the same time, all $CD44^+$ cells, which were characterized with their ability to accumulate NCs, had extremely high levels of their fluorescence, i.e., at the level of 1662 ± 33.89 arb. units. The data obtained indicate that only 17.14 ± 2.13% of EC cells, expressing the CD44, are capable of accumulating NCs. This subpopulation may certainly be CD44 cells, suggesting that tumor cells with stem potential (CD44 cells) may be the preferred target for the anti-proliferative properties of hybrid NCs.

One of the possible pathways of antitumor action of nanomaterials based on orthovanadate is to generate reactive oxygen species with subsequent mitochondrial function damage or induction of cell death by apoptosis/necrosis [15]. Therefore, at the end of each incubation period of cells with NPs and hybrid NCs (1–4 h), the activity indices of mitochondrial cell respiration were determined using the Cell Growth Determination Kit MTT based (Sigma, USA) according to the manufacturer's instructions, as well as the number of apoptotic and necrotic cells using annexin-V—An (BD, USA) and Propidium iodide—PI (Sigma, USA) on a FACS Calibur Becton–Dickinson flow cytometer.

According to the research results after the first hour of incubation of the EC cells with NPs and hybrid NCs, there was a tendency to a decrease in the level of mitochondrial respiration (Fig. 9); functions of NADP-H-dependent oxide reductase enzymes of mitochondria. After 2 h of incubation with NPs and hybrid NCs, the difference in control was statistically significant (by 20.5 and 27%, respectively). At the third hour of observation, the optical density of formazan solution in both types of treatment reached the minimum values, remaining at this level and at the fourth hour of incubation (optical density for NPs was 35.8 and hybrid NCs it made 46% if compared with control). That is, treatment of both by NPs and hybrid NCs for 3 h contributed to the maximum inhibition of mitochondrial respiration of EC cells.

The results suggest that inhibition of mitochondrial respiration through damage to the mitochondrial enzymatic system is an early sign of the toxic effect of nanomaterials used in the work in respect of EC cells, and this may subsequently lead to their death.

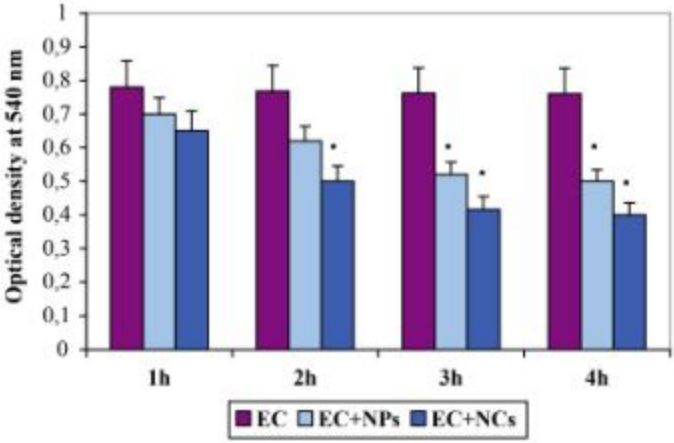

Fig. 9 Metabolic activity of EC cells before and after incubation with spherical NPs (**a**) and hybrid NCs (**b**) for 1, 2, 3 and 4 h. *Note* Asterisk—difference is statistically significant compared with similar indices of EC cells without incubation with NPs or hybrid NCs (control) ($p < 0.05$)

Mitochondria are considered the main link that integrates the various signals involved into implementation of apoptosis, the programmed cell death [15]. Simultaneous staining with annexin-V and PI allows the determination of the type of cell death. Annexin-V in the presence of Ca^{2+} and Mg^{2+} ions interact with phosphatidylserine, which at the early stages of apoptosis moves from the inner membrane of the cell to the outer. The living cell membrane is impermeable to PI. However, with irreversible damage to the cell (necrosis), the PI passes through the cell membrane and is capable of intercalation with defragmented DNA. Double staining with annexin-V and propidium iodide indicates late stages of apoptosis.

It has been found that in the control samples, regardless of incubation time, the number of living cells (An^-/PI^-) was $90 \pm 2.3\%$, those of early apoptosis (An^+/PI^-) made $1.34 \pm 0.67\%$, the ones of late apoptosis (An^+/PI^+) was $1.26 \pm 0.13\%$ and necrosis (An^-/PI^+) was $3.16 \pm 0.42\%$ (Fig. 10). Addition of both types of nanomaterials (NPs or hybrid NCs) to the EC cells resulted in a gradual decrease in the proportion of living cells (An^-/PI^-) throughout the observation period.

At the same time, from the first days of incubation, the difference in the effect of NPs or hybrid NCs on the type of cell death was noted. It has been shown that the addition of NPs to the EC cells after 1 h caused an increase in the amount of An^+/PI^- from 1.34% up to 6.11% ($p < 0.05$), which indicates the restructuring of the composition of membranes under the action of NPs and the beginning of the implementation of the mechanism of apoptotic cell death. In contrast, hybrid NCs were able to induce a statistically significant rise in the number of late-onset apoptosis (An^+/PI^+) and necrosis (An^-/PI^+) cells after 1 h of incubation (Fig. 10).

Further incubation of the cells with NPs (2–4 h) led to a gradual decrease in the proportion of cells in early apoptosis (An^+/PI^-) on the background of a rise in the

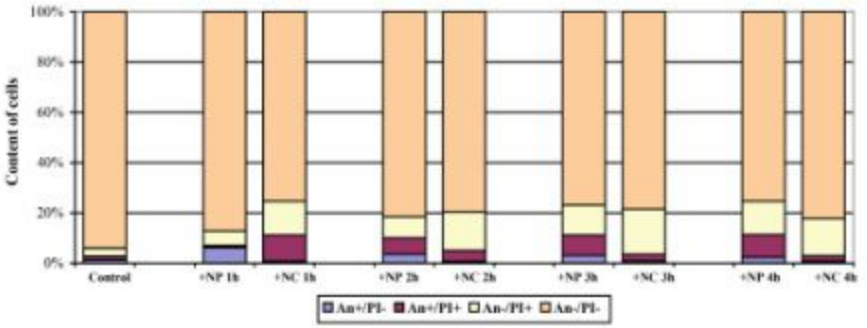

Fig. 10 The ratio of apoptotic/necrotic cells revealed with annexin-V/PI staining before and after incubation with spherical NPs (**a**) and hybrid NCs (**b**) for 1, 2, 3 and 4 h

percentage of cells in late apoptosis (An^+/PI^+) and necrosis (An^-/PI^+). It has been shown that 3 h after the start of incubation under the influence of NPs, the maximum redistribution of the number of cells in the apoptosis/necrosis occurs: the number of early apoptotic cells decreased by 2 times compared to 1 h of incubation, and the number of necrotic and late apoptotic cells increased by 2 and 7 times, respectively, compared to 1 h of treatment with NPs. Prolongation of the time of exposure of NPs to tumor cells up to 4 h did not lead to statistically significant differences in the ratio of the proportion of living, apoptotic and necrotic cells (Fig. 10). Thus, at the third hour of exposure to the NPs, the maximum cell death was observed by both necrosis and apoptosis with some advantage of the latter.

Thus, the data obtained suggest that NPs belong to those unique compounds that can simultaneously cause several types of cell death. Compounds which act in a similar manner are known [25]. The authors attribute this to simultaneous damage to both the inner and outer mitochondrial membranes. When the inner membrane is disrupted, the mitochondrial membrane potential changes, that is a prerequisite for cell death by necrosis. On the other hand, when the outer mitochondrial membrane is damaged, the cytochrome C is released, causing apoptosis. The above experimental data on mitochondrial dysfunction throughout the observation period indicate that hybrid NPs can act in the same way.

Regarding the effect of hybrid NCs on the EC cells, it has been established even starting from the first time of incubation and later throughout the observation period that the predominant tumor cell death was by necrosis. Moreover, within 1–4 h, a gradual increase in the percentage of necrotic cells (An^-/PI^+) was found compared to the control with maximum values reached after 3 h of incubation ($19.29 \pm 2.43\%$) (Fig. 10). In this case, the number of cells being in early apoptosis (An^+/PI^-) remained virtually unchanged within 1–4 h and did not differ significantly from the control values. Under the influence of hybrid NCs, the proportion of cells in late apoptosis (An^+/PI^+) was significantly increased by 1 h of incubation ($9.58 \pm 7.54\%$ compared

with 1.26 ± 0.13% in control). This index decreased rapidly throughout the observation period down to 2.79 ± 0.32% at the third hour, remaining at this level up to 4 h (2.06 ± 0.11%).

Thus, it draws attention to the fact that, in contrast to the effects of NPs, incubation of tumor cells with hybrid NCs for 3 h caused the highest cell death by necrosis and this was accompanied by a maximal decrease in metabolic activity of mitochondria. The established features of NPs or hybrid NCs on a cell death type are important for further development/inactivation of tumor in vivo.

It is believed that one of the reasons for ineffectiveness of the body's antitumor immune response and formation of immunological tolerance in malignant tumors is activation of cell death by apoptosis [26]. It is known that the apoptotic pathway of cell death leads to an activation of phagocytosis without consequences for the body in the form of alteration and inflammation [27]. In case of tumor cell death by necrosis, the release of DNA, RNA and tumor-specific proteins, which are DAMPs (damage-associated molecular patterns) and are recognized by the immune system, triggering a tumor-specific immune response. [28]. The release of DAMPs and cell death by necrosis leads to an activation of the TLR4 signaling pathway, which enhances the production of the transcription factor NF-kB, that resulted in an increased production of proinflammatory cytokines and development of immune-inflammatory process [29].

Therefore, depending on the method of cell death in the body of the tumor carrier can develop as an immune inflammative and immune-suppressive state. This demonstrates the need to review therapeutic strategies and target them to "switch" the mechanism of tumor cell death from apoptotic to necrotic. The above data indicate that hybrid NCs are capable of this task solving.

This assumption was experimentally confirmed in vivo by estimating the intensity of EC development from cells that had been pre-incubated with NPs and hybrid NCs for different times (1–4 h) (Table 2).

After 7 days of in vivo culturing of the EC cells of all the groups, inhibitory action of NPs and hybrid NCs was observed on an absolute number of EC cells in PC. However, only after 3-h incubation of both types of nanomaterials with EC cells, a statistically significant decrease in an absolute number of EC cells in PC (23.03 ± 4.87% in the NPs and 18.27 ± 1.23 in the hybrid NCs) compared to the control (55.09 ± 7.56%). The advantageous effect of nanocomplexes in minimizing the accumulation of tumor cells was noted, but first of all, in the group with the induction of EC cells, which had been pre-incubated with hybrid NCs for at least 3 h.

The decrease in an absolute number of the EC cells in PC (Table 2) under the action of nanomaterials in all the experimental groups indicates suppression of EC intensity growth. Judging by this index the hybrid NCs had a maximum antitumor effect. After 3-h of incubation, it was 33.16 ± 4.67%.

Thus, the data obtained indicate that only after 3 h of incubation of nanomaterials with the EC cells their significant antitumor effect was marked. With the same time of previous exposure to tumor cells (3 h), the hybrid NCs had some advantage over the use of just NPs.

Table 2 Intensity of growth of EC cells pretreated with spherical NPs and hybrid NCs for 1, 2, 3 and 4 h

Group	Volume of ascitic fluid (ml)	Number of EC cells in PC ($\times 10^7$)	Absolute number of EC cells in PC ($\times 10^7$)	Intensity growth of EC (%)
Control (EC cells)	5.84 ± 0.77	9.54 ± 1.55	55.09 ± 7.56	100
EC + NPs 1 h	4.4 ± 0.56	12.00 ± 2.03	51.14 ± 9.87	92.82 ± 5.65
EC + NPs 2 h	4.26 ± 0.85	10.23 ± 1.38	43.57 ± 6.71	79.10 ± 4.38
EC + NPs 3 h	3.08 ± 1.02	7.48 ± 2.09	23.03 ± 4.87*	41.80 ± 3.54
EC + NPs 4 h	2.62 ± 0.71	10.89 ± 1.90	27.58 ± 7.87*	49.06 ± 2.78
EC + NCs 1 h	4.5 ± 0.64	11.10 ± 0.84	49.5 ± 3.74	89.85 ± 4,87
EC + NCs 2 h	3.8 ± 0.72	10.75 ± 0.94	40.66 ± 5.41	73.81 ± 3,23
EC + NCs 3 h	2.9 ± 0.43	6.37 ± 0.72	18.27 ± 1.23*	33.16 ± 4,67
EC + NCs 4 h	3.1 ± 0.27	5.68 ± 0.64	17.6 ± 1.58*	31.95 ± 3,89

Notes An absolute number of EC cells in PC was found by the formula: ANC = Vol * Conc, where Vol is the volume of ascites fluid in PC of animals (ml), Conc is the concentration of tumor cells counted in Goryaev's chamber ($\times 10^7$ cells/ml)

Intensity growth of EC (I) was calculated by the formula: I = [(ANC (experiment)/ANC (Control)] * 100%, where ANC (experiment) is the absolute number of tumor cells in PC of animals with EC, which was initiated by treated nanomaterial cells; ANC (Control) is the absolute number of cells in PC of animals with EC, which was initiated by untreated nanomaterial cells

Thus, successful implementation of antitumor ability of hybrid NCs involves the implementation of a multi-stage cascade, namely, their penetration, accumulation inside cells, impaired mitochondrial function with subsequent induction of apoptotic and necrotic changes. There is absolutely no possibility of existence of "alternative" mechanisms for the implementation of the antitumor action of hybrid NCs. As we established in our previous studies, the treatment of EC cells with hybrid NCs led to the formation of a pool of tumor cells with reduced expression of pluripotency genes, primarily *nanog*, which is key in determining the self-support of cancer stem cells [30]. In general, the obtained results complement the understanding of the mechanisms of implementation of anticancer therapy of nanomaterials based on rare-earth orthovanadates.

4 Conclusions

1. In experimental conditions in vivo the possibility of using $GdYEuVO_4$ nanoparticles and hybrid nanocomplexes synthesized on their basis for the identification of cancer cells and inhibition of tumor growth is substantiated, that allows attributing these nanomaterials to promising drugs for the diagnosis and treatment of malignancies.

2. The dependence of an antitumor effect of nanomaterials on the time of their pre-incubation with tumor cells was established. Treatment of EC cells in vitro with hybrid nanocomplexes within 3 h resulted in a minimal EC intensity growth in vivo (33.16 ± 4.67%).
3. Implementation of an antitumor effect of nanomaterials involves their penetration, accumulation inside tumor cells, damage to mitochondrial function with subsequent induction of apoptotic and necrotic changes. The established fact of the death of EC cells mainly by necrosis under the action of hybrid NCs is one of the conditions for further inactivation of a tumor.
4. Double staining of EC cells with monoclonal antibodies to CD44, together with hybrid NCs, allowed them to establish their selective accumulation capacity in $CD44^+$ EC cells with ultra-high fluorescence intensity of this marker (CD44 cells). This confirms that a successful implementation of anti-proliferative properties of hybrid NCs is accomplished by inhibiting the function of tumor cells with a stem potential.

References

1. World Health Organization (2018) Global status report on noncommunicable diseases 2018. WHO Press, Geneva
2. Hirsch LR, Stafford RJ, Bankson JA et al (2003) Nanoshell-mediated near-infrared thermal therapy of tumors under magnetic resonance guidance. PNAS 100:13549–13554
3. Liu X, Tao H, Yang K et al (2011) Optimization of surface chemistry on single-walled carbon nanotubes for in vivo photothermal ablation of tumors. Biomaterials 32:144–151. https://doi.org/10.1016/j.biomaterials.2010.08.096
4. Du X, Lin WC, Su HH (2019) Highly efficient polyethylene glycol-functionalised gold nanorods for photothermal ablation of hepatocellular carcinoma cells. IET Nanobiotechnol 13(8):842–849. https://doi.org/10.1049/iet-nbt.2018.5417. PMID: 31625525
5. Xu L, Wang SB, Xu C et al (2019) Multifunctional albumin-based delivery system generated by programmed assembly for tumor-targeted multimodal therapy and imaging. ACS Appl Mater Interfaces 11(42):38385–38394. https://doi.org/10.1021/acsami.9b11263
6. Karpenko NA, Malukin YV, Koreneva EM et al (2013) The effects of chronic intake of nanoparticles of cerium dioxide or gadolinium ortovanadate into aging male rats. In: Proceedings of the 3rd international conference «Nanomaterials: applications and properties '2013». Alushta, Ukraine, 2(4):04NAMB28-1–04NAMB28-4
7. Rozzo C, Sanna D, Garribba E et al (2017) Antitumoral effect of vanadium compounds in malignant melanoma cell lines. J Inorg Biochem 174:14–24. https://doi.org/10.1016/j.jinorgbio.2017.05.010
8. Leon IE, Cadavid-Vargas JF, Di Virgilio AL, Etcheverry SB (2017) Vanadium, ruthenium and copper compounds: a new class of nonplatinum metallodrugs with anticancer activity. Curr Med Chem 24:112–148. https://doi.org/10.2174/0929867323666160824162546
9. Štefančíková L, Lacombe S, Salado D et al (2016) Effect of gadolinium-based nanoparticles on nuclear DNA damage and repair in glioblastoma tumor cells. J Nanobiotechnol 14(1):63. https://doi.org/10.1186/s12951-016-0215-8
10. Klochkov VK, Kavok NS, Maljukin JV, Seminozhenko VP (2010) Jeffekt specificheskogo vzaimodejstvija nanokristallov GdYVO4:Eu3 + s jadrami kletok. Dopovidi Nacional'noï akademiï nauk Ukraïni 10:81–86 [Ukrainian]

11. Dabros W, Nikiforuk A, Kordowiak AM (2004) The influence of bis(kojato)-oxovanadium (IV) on viability and proliferation of rat hepatoma cell line H 35-19. In: ELSO proceedings NICE, France Abstract no. 653, p 299
12. Kordowiak AM, Klein A, Goc A, Dabroś W (2007) Comparison of the effect of $VOSO_4$, Na_3VO_4 and $NaVO_3$ on proliferation, viability and morphology of H35-19 rat hepatoma cell line. Pol J Pathol 58(1):51–57
13. Rodrguez-Mercado JJ, Mateos-Nava RA, Altamirano-Lozano MA (2011) DNA damage induction in human cells exposed to vanadium oxides in vitro. Toxicol In Vitro 25:1996–2002. https://doi.org/10.1016/j.tiv.2011.07.009
14. Molinuevo MS, Barrio DA, Cortizo AM, Etcheverry SB (2004) Antitumoral properties of two new vanadyl (IV) complexes in osteoblasts in culture: role of apoptosis and oxidative stress. Cancer Chemother Pharmacol 53(2):163–172
15. Korbecki J, Baranowska-Bosiacka I, Gutowska I, Chlubek D (2012) Biochemical and medical importance of vanadium compounds. Acta Biochim Pol 59(2):195–200
16. Klochkov VK (2015) Method for producing water dispersion of cholesterol. Patent of Ukraine 108011 [Ukrainian]
17. Al – Jarallah A, Trigatti BL (2010) A role for the scavenger receptor, class B type I in high density lipoprotein dependent activation of cellular signaling pathways. Biochim Biophys Acta 1801(12):1239–1248. https://doi.org/10.1016/j.bbalip.2010.08.006
18. Klochkov VK (2009) Aqueous colloid solutions of nanoluminophores nReVO4:Eu3+ (Re = Y, Gd, La). Mater Sci Nanostruct 2:3–8 [Ukrainian]
19. Klochkov VK, Grigorova AV, Sedyh OO, [i dr.] (2012) Harakteristiki zolej nReVO4:Eu3+ (Re = La, Gd, Y, Sm) s nanochasticami raznoj formy i razmerov. ZhPS 79(5):738–742 [Ukrainian]
20. Malyukina M Yu, Piliai I.V, Sedih OO, [i dr.] (2018) Aggregation stability of nanoparticles based on rare-earth elements in different microenvironment and biological media. Biophys Bull 40:5–16 [Ukrainian]
21. Ozaslan M, Karagoz ID, Kilic IH, Guldur ME (2011) Ehrlich ascites carcinoma. Afr J Biotechnol 10(13):2375–2378
22. Goltsev AN, Babenko NN, Gaevskaya YA et al (2017) Nanotechniques inactivate cancer stem cells. Nanoscale Res Lett 12(1):415. https://doi.org/10.1186/s11671-017-2175-9
23. Goltsev AN, Babenko NN, Gaevskaya YA et al (2013) Capability of orthovanadate-based nanoparticles to in vitro identification and in vivo inhibition of cancer stem cells. Nanosystems Nanomaterials Nanotechnol 11(4):729–739 [Ukrainian]
24. Klochkov V, Kavok N, Grygorova G et al (2013) Size and shape influence of luminescent orthovanadate nanoparticles on their accumulation in nuclear compartments of rat hepatocytes. Mater Sci Eng C Biol Appl 33(5):2708–2712. https://doi.org/10.1016/j.msec.2013.02.046
25. Arakawa S, Nakanomyo I, Kudo-Sakamoto Y et al (2015) Identification of a novel compound that inhibits both mitochondria-mediated necrosis and apoptosis. Biochem Biophys Res Commun 467(4):1006. https://doi.org/10.1016/j.bbrc.2015.10.022
26. Fulda S (2013) Regulation of cell death in cancer - possible implications for immunotherapy. Front Oncol 3:29. https://doi.org/10.3389/fonc.2013.00029
27. Nagata S, Tanaka M (2017) Programmed cell death and the immune system. Nat Rev Immunol 17(5):333–340. https://doi.org/10.1038/nri.2016.153
28. Sathianathen NJ, Krishna S, Anderson JK et al (2017) The current status of immunobased therapies for metastatic renal-cell carcinoma. Immunotargets Ther 6:83. https://doi.org/10.2147/ITT.S134850
29. Luo J-L, Kamata H, Karin M (2005) IKK/NF-κB signaling: balancing life and death – a new approach to cancer therapy. J Clin Invest 115(10):2625. https://doi.org/10.1172/JCI26322
30. Goltsev AN, Babenko NN, Gayevskaya YuA et al (2015) Antitumor effect of hybrid nanocomplexes containing nanoparticles of orthovanadates rare earth elements and cholesterol. Genes Cells 10(2):54–60 [Russian]